

Tunneling spectroscopic signatures of charge doping and Mott-phase transition in α -RuCl₃ in proximity to graphite

Xiaohu Zheng^{1,2*}, Ke Jia³, Xingjun Wu¹, Youguo Shi³, Katsumi Tanigaki¹, Rui-Rui Du^{2,4}

¹Beijing Academy of Quantum Information Sciences, Beijing 100193, China.

²International Center for Quantum Materials, School of Physics, Peking University, Beijing 100871, China.

³Beijing National Laboratory for Condensed Matter Physics and Institute of Physics, Chinese Academy of Sciences, Beijing 100190, People's Republic of China.

⁴CAS Center for Excellence in Topological Quantum Computation, University of Chinese Academy of Sciences, Beijing 100190, China.

*Correspondence to: zhengxh@baqis.ac.cn

Introduction. Layered Mott insulator α -RuCl₃ has been intensely investigated as a possible candidate for Kitaev quantum spin liquid. In this letter, we report electron tunneling measurements on few-layer α -RuCl₃ in proximity to graphite, using a scanning tunneling microscopy. Signatures of charge doping have been observed in α -RuCl₃ layers stacking on the surface of graphite. Upon charge doping, we observed characteristic tunneling spectra that are dependent on the number of layers of α -RuCl₃. For a single α -RuCl₃ layer that is in direct contact with graphite, data shows charge states emerging in the Mott-gap regime with conservation of the Hubbard bands. For a bilayer of α -RuCl₃, data indicates an unconventional Mott-phase transition, where the Hubbard bands collapse accompanied by a dramatical gap-reduction. The results have thus demonstrated that tunneling into doped few-layer α -RuCl₃ is a useful probe to

investigate this otherwise insulating spin-liquid candidate, providing fundamental information concerning electronic properties and theoretically proposed strong correlation physics in α -RuCl₃.

Introduction. Kitaev quantum spin liquid (QSL) is a theoretical model for a strongly correlated spin phase. Its exact solution predicts the existence of Majorana zero modes (MZM) that obey non-Abelian statistics, a property that may offer a route towards fault-tolerant quantum computation [1,2]. A layered Mott insulator α -RuCl₃ has been intensely investigated as a possible candidate for Kitaev QSL [3–8]. The fingerprint for Majorana fermions of the fractionalized spin excitations in α -RuCl₃ has been reported by several experimental groups [9–11]. In particular, the recent observations of thermal Hall conductance with half-integer quantization have provided the key evidences for the chiral edge modes of charge neutral Majorana fermions [12–20]. On the other hand, the roadmap developed for the quantum technology platforms usually rely on electronic methods to manipulate the quantum bits [21]. The chargeless character of the quasiparticles and the electrically insulating nature of materials in the Kitaev QSL, such as α -RuCl₃, would generally limit the range of suitable electronic measurement techniques. Recently, several experiment setups in heterostructures comprised of conducting or superconducting films [22–31], which may access electronic signatures of the quantum excitations in Kitaev QSL, have been theoretically proposed. Moreover, the doped Kitaev models are thought to host a number of exotic quantum phases, in particular, a p-wave superconductor [32–34], which makes the research on charge

doping in Kitaev QSL more attractive and urgent. On the experimental side, however, this topic has remained largely unexplored.

In this Letter, we report the measurements of morphologies and surface electronic density of states on α -RuCl₃ flakes transferred onto a highly-oriented pyrolytic graphite (HOPG) substrate (see methods in Supporting Information), using scanning tunneling microscopy and spectroscopy (STM/STS) at liquid nitrogen temperature (77K). The signatures of charge doping and Mott-phase transition in α -RuCl₃/HOPG can be observed from analyzing the dI/dV spectra. Upon charge doping, new surface density of states (DOS) arise in the first α -RuCl₃ layer directly contacting to graphite owing to the overlap of electron orbitals between graphite and α -RuCl₃. Remarkably, the second α -RuCl₃ layer shows an entirely different surface DOS, where an unconventional Mott-phase transition is observed with a reduction in the bandgap. It suggests that the doped itinerant carriers and strong spin fluctuation together lead to a new correlated phase. These results provide general electronic information of α -RuCl₃ with proximity contact to graphite, and may pave the way for investigating strong correlation physics in α -RuCl₃.

Results and discussions. α -RuCl₃ is an insulating $4d$ transition-metal halide with honeycomb layers composed of nearly ideal edge-sharing RuCl₆ octahedra [35,36]. It is similar to graphite and can be easily exfoliated into a truly two-dimensional magnet. The magnitude and nature of the bandgap, however, still remain controversial; for example, the gap values are reported to range from 0.2 to 1.9 eV depending on employed methods [7,8,37,38]. In Fig. 1a, an atomically-resolved STM morphology

image was acquired on an α -RuCl₃ flake with thickness larger than 5 nm, which can provide information related to the bulk. Honeycomb shape Ru-lattice with some defects can be clearly observed in Fig. 1a. The lattice constant shown in the bottom panel is approximately 6.1 Å, which is consistent with the previous reports [36]. The averaged dI/dV signal measured at 77 K, far above the Néel temperature ($T_N \sim 7\text{K}$) [11], reveals a large insulating U-shaped bandgap of ~ 1.8 eV. This is in strong contrast to the calculations without considering spin correlations, which shows almost no gap with a paramagnetic phase for α -RuCl₃ [8]. It suggested that strong spin correlations, *i.e.* Kitaev interactions that can survive at a temperature higher than 100 K [11], should be involved. The bulk α -RuCl₃ is a spin-orbital assisted Mott insulator in Kitaev paramagnet phase [3], where the sharp conduction and the valence band observed in the spectra correspond to the upper and the lower Hubbard bands (UHB and LHB). The size of our measured bandgap is consistent with the optically measured values [7]. It is also consistent with the local density approximation (LDA) calculations where the zigzag magnetic order with strong spin-orbit coupling (SOC) and on-site Coulomb interaction U are considered [7,39]. Overall our tunneling experiment results have clearly revealed the strong correlations and Mott insulating nature of the bulk α -RuCl₃ [8,38].

As described in [32–34], charge transfer occurs when heterostructure is made between single-layer α -RuCl₃ and graphene, and thus such a heterostructure can be considered as a Kondo-Kitaev lattice, which may host certain exotic quantum phases. Here, we use HOPG as the substrate, which transfers charges to the above α -RuCl₃

layers more effectively. We find a region, as shown in Fig. 1c, where α -RuCl₃ single-layer (denote as 1: α -RuCl₃), bilayer (2: α -RuCl₃) and the HOPG can be observed simultaneously in a broad-view STM image. The height-profile between the single-layer and the bilayer α -RuCl₃ was about 600 pm (upper panel in Fig. 1d), which agrees well with the expected thickness of α -RuCl₃ monolayer with van der Waals interlayer coupling [5,40]. We note, however, the thickness of the single-layer α -RuCl₃ on graphite is only 350 pm, far below the predicted value [5,40]. It suggests that the contact between graphite and α -RuCl₃ is stronger than general van der Waals coupling. The measured dI/dV spectra in the selected area are collected as shown in the atomic-resolved STM image, across 1: α -RuCl₃ and 2: α -RuCl₃ (Fig. 1e). LDOSs on 1: α -RuCl₃ are remarkably inhomogeneous, where dI/dV spectra with U-sharped bandgap (~ 1.8 eV), V-shaped gapless LDOS and the intermediate states can be observed as changing the measuring positions, as selected shown in Fig. 1f. Characteristically, according to the dI/dV spectra on 2: α -RuCl₃, the Mott-gap is commonly reduced (~ 150 meV) over the bulk value. Compared with the bulk dI/dV spectra in Fig. 1b, the tunneling signatures in Fig. 1f suggest that significant modifications of the electronic states, including Mott-phase transition, take place in doped α -RuCl₃ and the modified electronic states are greatly layer-dependent.

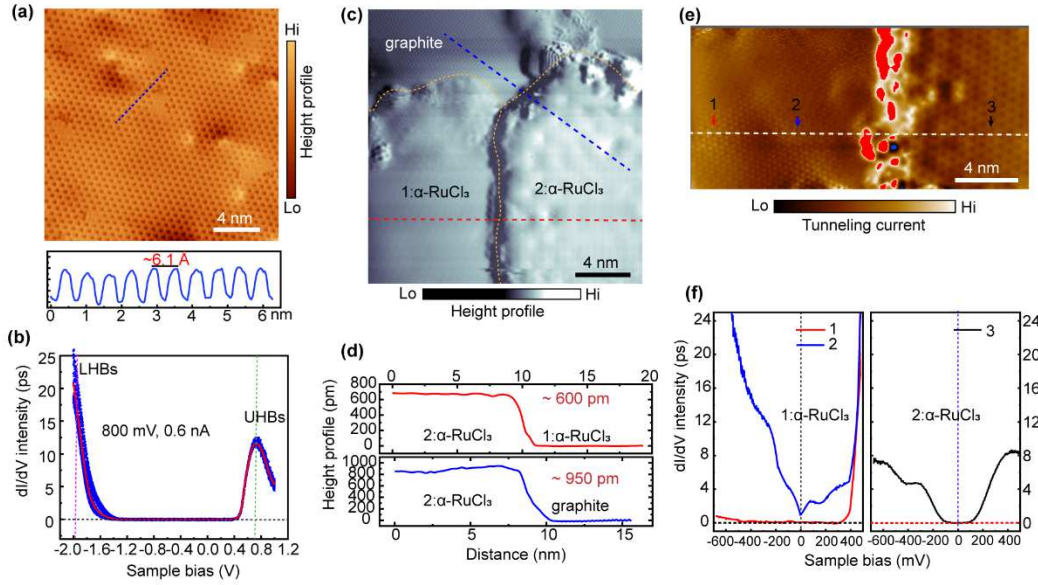


Fig. 1. (a) Upper panel: STM morphology of α - RuCl_3 (>5 layers) transferred onto HOPG; Bottom panel: cross-sectional profile along the blue line shows the lattice constant is 6.1 \AA ; (b) Averaged dI/dV spectra with clear bandgap of about $1.8 \text{ eV} \pm 0.2 \text{ eV}$ acquired over a wide region in (a) at 77 K (sample voltage=800 mV; setpoint=0.6 nA); (c) Broad view STM image shows a region that the graphite substrate covered by signal and bilayer α - RuCl_3 domains (denoted as 1: α - RuCl_3 and 2: α - RuCl_3); (d) step profiles acquired between 2: α - RuCl_3 and 1: α - RuCl_3 , 2: α - RuCl_3 and graphite; (e) high-resolution STM image across 1: α - RuCl_3 and 2: α - RuCl_3 shows the apparent difference of atoms arrangement; (f) selected dI/dV curves as marked in (e) shows the huge difference of surface LDOS in α - RuCl_3 (sample voltage=500 mV, setpoint=500 pA).

To understand the electronic structures of α - RuCl_3 , we firstly focused on the LDOS on the first layer that directly contacts with graphite. A region as shown in Fig. 2a was captured, where the α - RuCl_3 lattices is locally distorted by strain introduced during transfer process. The tunneling spectra along the blue line in Fig. 2a show a smooth

evolution of Mott-gap collapse approaching to the strain center, as shown in Fig. 2b. In the beginning, the spectra show a Mott-gap comparable to the bulk and it is very sensitive to the strain, as shown in the following. The intensity of the valence band gradually increases toward the Fermi level accompanied with a new hole state emerging peaked at ~ 600 meV, as the tip approaches to the strain center from both sides (Fig. S1). Notice there is a negligible change of the UHB in the conduction band. The Mott-gap is suppressed from a U shape to a V one at the Fermi level, and finally develops together with a finite LDOS, representing a metallic state with both hole and electron density inside the gap. Similar strain-induced evolution of dI/dV spectra were reported in [41–43] concerning the Mott-phase transition for other two-dimensional compounds. In this work, however, we carefully checked the strained region on multi-layers α - RuCl_3 (bulk states), but similar Mott-gap collapse was not observed, which excludes the possibility that the Mott-gap collapsing purely results from the strain. Here is another notable phenomenon that the lattice acquired in the strain region show huge deviation from the lattice of α - RuCl_3 (Fig. 2a).

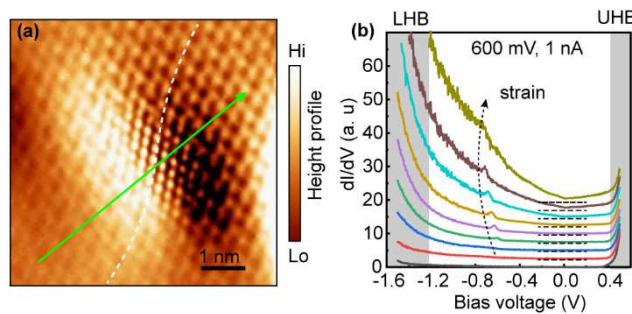


Fig. 2. (a) atomic resolved STM image on 1: α - RuCl_3 , where the strain distorts the lattice along the dashed white line; (b) selected dI/dV spectra show a clear evolution of LDOS as the measurements approach to the strain center, where the insulating spectra evolves

into metallic form with a peaked DOS emerge around -600 meV (sample voltage=600 mV, setpoint=1 nA)

To fully understand the electronic structure in the first α -RuCl₃ layer on graphite, an atomic-resolved STM image as a function of the sample voltage (V_H) and setpoint current (I_s) were collected in the same region. As shown in Fig. 3a, under a high V_H and a low I_s (large tip-surface distance d_s), the lattice of α -RuCl₃ can be observed clearly. In decreasing d_s by either decreasing V_H or increasing I_s , the lattice structure of the STM morphology image gradually evolves into a smaller honeycomb form that is similar to graphene's lattice. The evolution is very sensitive to strain and preferentially occurs in regions with lattice distortion, which well explains the variations of dI/dV spectra in the first α -RuCl₃ layer in Fig. 1f. When V_H is lower than 500 mV with $I_s = 1$ nA, the lattice constant and orientation are entirely consistent with those of the underneath graphite (Fig. S2), which demonstrates the tunneling signals are closely related to graphite's orbitals. However, V_H applied on the sample is still above the Mott-gap, where the electrons residing in the UHB in α -RuCl₃ may contribute to the tunneling signals.

To observe the dI/dV spectra corresponding to the STM image's evolution, we performed d_s dependent STS in the region without strain. During the measurements of dI/dV spectra, V_H and I_s were set to hold the tip on the surface with a constant distance d_s as shown in the inset in Fig. 3c, and the dI/dV spectra can be collected by sweeping the sample bias. The tip-surface distance d_s can be calculated using the formula: $d_s =$

$$-\frac{\hbar}{2\sqrt{2m\Phi}} \ln\left(\frac{R_0 I_s}{V_H}\right),$$

where m is the mass of the tunneling electron, Φ is the average work

function of the tip and the sample, R_0 is the resistance for a single-atomic point contact [44]. In Fig. 3b, we provide the dI/dV spectra at a fixed setpoint of 1 nA. By increasing the V_H , *ie.* decreasing d_s , a new state at ~ -1.3 eV emerges above the LHB together with a small shift of the band edge to the Fermi level. At $V_H = 450$ mV, we observed another DOS peak at -600 meV as the same as the strain induced peak in Fig. 2b. The gap is reduced in these new states emerging in the valence band. When V_H is below 450 mV, the gap is completely closed with V-shaped LDOS at the Fermi level. However, both the UHB and LHB are still observable, which means the ground state is still in Mott-phase with strong on-site Coulomb repulsion, even in the gapless condition.

To distinguish the V-shaped LDOS from the Dirac-point in graphene, we carefully compared the spectra in Fig. S3. A negatively shifted Dirac-point belonging to graphite was observed, when V_H moves into the Mott-gap ($V_H = 400$ mV) and the underneath graphite can be seen through the α -RuCl₃ signal layer more easily (Fig. S3). The shift of the graphene's Dirac-point reveals a work function-mediated interlayer charge transfer at the graphene/ α -RuCl₃ heterostructure interface [45,46]. We also performed measurements of dI/dV spectra at a fixed V_H with increasing I_s , which also well show states emerging above LHB inside the gap (Fig. S4). It means that the gap states revealed in dI/dV spectra are mainly selectively detected by d_s , not individually by V_H . But whether they are truly surface states of the heterostructure or new states induced by tip-surface interactions, such as tip induced electric field as decreasing d_s , is still puzzling?

To answer this question, we fitted the dI/dV intensity of the arising LDOS peak at

-1350 meV over the tip-surface distance in the framework of the Tersoff and Hamann's tunneling formalism [47]: $\frac{dI}{dV} \propto e^{-2kd_s} N(eU_{bias})$, where k is the constant, $d_s = -\frac{\hbar}{2\sqrt{2m\Phi}} \ln\left(\frac{R_0 I_s}{V_H}\right)$, and $N(eU_{bias})$ is the surface density of states at a certain bias voltage U_{bias} . The formula, using the constant parameters and without considering any effects relating to the tip, well describes the decay length of the wave functions on the measured surface. As shown in Fig. 3c, the evolution of dI/dV peak intensity over the tip-surface distance fits perfectly. It demonstrates that the states to collapse the Mott-gap are ever-present with a short decay length, and not newly raised as decreasing d_s . Instead, they can be detected only when the tip is close to the surface (as schematically shown inset in Fig. 3c). In general, the results in Fig. 3 clearly provide such information that hybridization of electron wavefunctions between α -RuCl₃ and graphite induces the states in the Mott-gap.

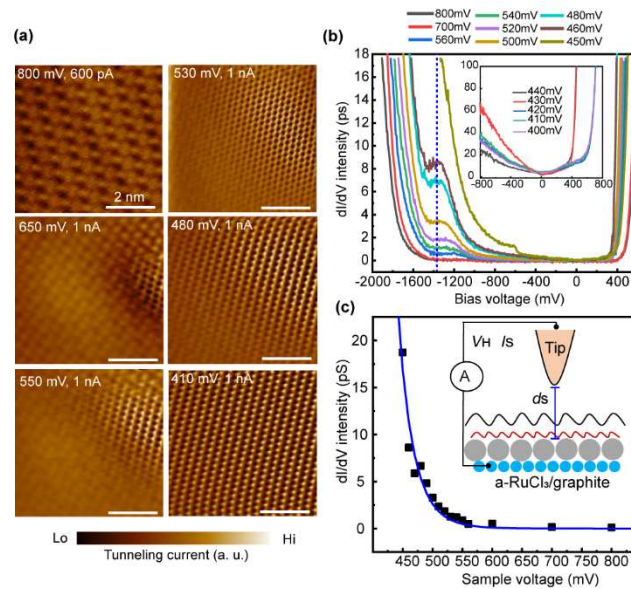


Fig. 3. (a) STM images acquired on 1: α -RuCl₃ with variation of the sample voltage show the topographic evolution that the lattice turns from α -RuCl₃ into the graphite; (b) dI/dV spectra on 1: α -RuCl₃ acquired as variation of the tip-surface distance by changing

sample voltage with a fixed setpoint current of 1 nA; **(b)** Peak intensity at -1350 meV as a function of sample voltage is fitted using the distance-dependent Tersoff and Hamann's tunneling formalism [47]. Inset schematically shows the experimental setup when dI/dV are performed, where the orbital can be selectively detected by changing the tip-surface distance.

An interesting question arise: does charge transfer occur for the second layer? And furthermore, if so, is charge transfer a precursor for new electronic phase? We examined the tunneling spectra in the second α -RuCl₃ layer that doesn't directly contact to graphite. Fig. 4a shows a different region compared to that in Fig. 1c with the height profile of about 1 nm. The atomic-resolved STM image shows honeycomb with a lattice constant of ~ 6.2 Å, similar to the bulk but with a small distortion. The tunneling spectra along the white arrow line in Fig. 4a across both α -RuCl₃ and graphite areas show stable and typical V-shaped curve at the Fermi level on graphite (Fig. 4c). In comparison to the spectra in bulk and the first α -RuCl₃ layer, the second α -RuCl₃ layer shows that the framework of the Mott-phase is destroyed with an unconventional phase transition, where the Hubbard bands disappear and a large Mott-gap evolves into reduced gap (~ 150 meV) with two well-resolved shoulder peaks on both sides (Figs. 4c and d). The gap magnitude in the newly emergent phase is stable over the surface and the spectrum curve is qualitatively the same as that collected in a different region in Fig. 1f, demonstrating a universal nature of the second α -RuCl₃ layer above graphite. There is negligible tip-surface distance and strain dependent dI/dV behaviors, which is entirely

different from the case in the single-layer. A similar Mott-phase transitions were previously observed by APRES [10] in rubidium doped α - RuCl_3 , where the Mott gap is also suddenly reduced into a new gapped phase under ionic doping. The phase transition is interpreted to be the correlation between doping-charges and strong spin fluctuation, where the Mott-insulator evolves into a correlation band insulator.

Although the gap is very stable in the dI/dV spectra at the position far away from the step, modulation is clear on the shoulder peak in the valence band. The dI/dV spectra from bright zone (A) to dark zone (B) in Fig. 4b has been collected. In Fig. 4d, we can see that the intensity of filled states prominently increases as the STM tip moves from A to B, which indicates an accumulation of holes in the dark zone (B), whereas no obvious change occurs in empty states. The corresponding modulation of surface LDOS can be more clearly seen in the energy-resolved dI/dV maps at constant tip-sample separation, as shown in Fig. 4e. The dI/dV maps at negative biases display a similar pattern, where high intensity LDOS is concentrated in the dark zones of the morphology images in Fig. 4b. Whereas, the distribution of LDOS at positive biases is reversed with slightly higher intensity LDOS in the bright zones of the morphology image. In addition, we didn't see any clear atomic lattice revealed in the dI/dV maps at energy levels in either the conduction band or the valence band, suggesting that the charges in the second α - RuCl_3 layer are itinerant rather than localized in atomic orbitals.

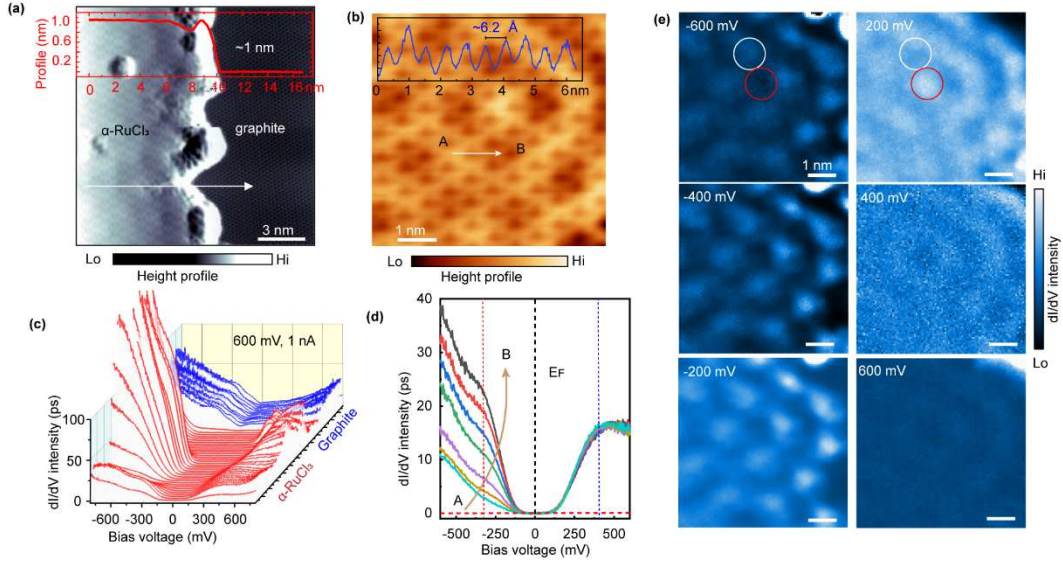


Fig. 4. (a) a broad view STM image of α -RuCl₃ on graphite, inset the height profile shows the thickness is about 1 nm; (b) high-resolved STM image shows the lattice is periodically modulated into bright and dark zones, and the lattice constant is ~ 6.2 Å; (c) dI/dV spectra acquired along the white line across α -RuCl₃ and graphite in (a) (sample voltage=600 mV, setpoint=1 nA); (d) selected dI/dV spectra from bright (A) to dark zones (B) shows the significantly increasing of the valence band; (e) dI/dV spectroscopic maps corresponding to the topology in (b) as variation of the bias voltage labelled in the images.

Conclusion. In conclusion, the signatures of charge transfer and accumulation, and Mott-phase transition in α -RuCl₃ were directly observed from the dI/dV spectra. A crossover from gapped to metallic dI/dV spectra has been detected in single-layer α -RuCl₃ that is directly contacting to graphite, by the measurement being across the distorted lattice. By approaching the STM tip to the surface, we observed density of states that are associated with graphite and decay fast into the vacuum, in the Mott-gap

regime. It presents the overlap of wavefunctions between graphite and α -RuCl₃, which provides visible evidence for the charge transfer to α -RuCl₃ in the heterostructure. However, the framework of Hubbard bands is still observable, thus demonstrating that there is no Mott-phase transition in the signal-layer α -RuCl₃. On the other hand, unconventional Mott-phase transition with collapse of Hubbard bands and decrease of the gap size was observed on the second α -RuCl₃ layer. Itinerant carriers transferred to the bilayer α -RuCl₃ are considered to lead to a new electron-correlated phase. The results demonstrate intriguing electronic phenomenon in doped α -RuCl₃ Kitaev QSL system, which warrants future theoretical and experimental investigations.

Acknowledgments. We thank Deepak Karki for useful discussion. This work was supported by National Basic Research & Development plan of China (Grants No. 2019YFA0308400), the National Natural Science Foundation of China (Grants No. U2032204), and the Strategic Priority Research Program of the Chinese Academy of Sciences (Grants No. XDB28000000 and XDB33030000).

References

- [1] A. Kitaev, *Anyons in an Exactly Solved Model and Beyond*, Ann. Phys. **321**, 2-111 (2006).
- [2] A. Yu. Kitaev, *Fault-Tolerant Quantum Computation by Anyons*, Ann. Phys. **303**, 2-30 (2003).
- [3] K. W. Plumb, J. P. Clancy, L. J. Sandilands, V. V. Shankar, Y. F. Hu, K. S. Burch, H.-Y. Kee, and Y.-J. Kim, *α -RuCl₃: A Spin-Orbit Assisted Mott Insulator on a Honeycomb Lattice*, Phys. Rev. B **90**, 041112 (2014).
- [4] Y. Kubota, H. Tanaka, T. Ono, Y. Narumi, and K. Kindo, *Successive Magnetic Phase Transitions in α -RuCl₃: XY-like Frustrated Magnet on the Honeycomb Lattice*, Phys. Rev. B **91**, 094422 (2015).
- [5] H. B. Cao, A. Banerjee, J.-Q. Yan, C. A. Bridges, M. D. Lumsden, D. G. Mandrus, D. A. Tennant, B. C. Chakoumakos, and S. E. Nagler, *Low-Temperature Crystal and Magnetic Structure of α -RuCl₃*, Phys. Rev. B **93**, 134423 (2016).
- [6] A. Koitzsch, C. Habenicht, E. M ueller, M. Knupfer, B. Buechner, H. Kandpal, J.

- van den Brink, D. Nowak, A. Isaeva, and T. Doert, *J_{eff} Description of the Honeycomb Mott Insulator α -RuCl₃*, Phys. Rev. Lett. **117**, 126403 (2016).
- [7] S. Sinn et al., *Electronic Structure of the Kitaev Material α -RuCl₃ Probed by Photoemission and Inverse Photoemission Spectroscopies*, Sci. Rep. **6**, 39544 (2016).
- [8] X. Zhou, H. Li, J. A. Waugh, S. Parham, H.-S. Kim, J. A. Sears, A. Gomes, H.-Y. Kee, Y.-J. Kim, and D. S. Dessau, *Angle-Resolved Photoemission Study of the Kitaev Candidate α -RuCl₃*, Phys. Rev. B **94**, 161106 (2016).
- [9] S.-H. Baek, S.-H. Do, K.-Y. Choi, Y. S. Kwon, A. U. B. Wolter, S. Nishimoto, J. van den Brink, and B. Büchner, *Evidence for a Field-Induced Quantum Spin Liquid in α -RuCl₃*, Phys. Rev. Lett. **119**, 037201 (2017).
- [10] A. Banerjee, J. Yan, J. Knolle, C. A. Bridges, M. B. Stone, M. D. Lumsden, D. G. Mandrus, D. A. Tennant, R. Moessner, and S. E. Nagler, *Neutron Scattering in the Proximate Quantum Spin Liquid α -RuCl₃*, Science **356**, 1055 (2017).
- [11] S.-H. Do et al., *Majorana Fermions in the Kitaev Quantum Spin System α -RuCl₃*, Nat. Phys. **13**, 1079-1084 (2017).
- [12] Y. Kasahara, S. Suetsugu, T. Asaba, S. Kasahara, T. Shibauchi, N. Kurita, H. Tanaka, and Y. Matsuda, *Quantized and Unquantized Thermal Hall Conductance of Kitaev Spin-Liquid Candidate Majorana Fermions in the Kitaev Quantum Spin System α -RuCl₃*, ArXiv220211947 Cond-Mat (2022).
- [13] T. Yokoi et al., *Half-Integer Quantized Anomalous Thermal Hall Effect in the Kitaev Material Candidate α -RuCl₃*, Science **373**, 568 (2021).
- [14] Y. Kasahara et al., *Unusual Thermal Hall Effect in a Kitaev Spin Liquid Candidate α -RuCl₃*, Phys. Rev. Lett. **120**, 217205 (2018).
- [15] Y. Kasahara et al., *Majorana Quantization and Half-Integer Thermal Quantum Hall Effect in a Kitaev Spin Liquid*, Nature **559**, 7713 (2018).
- [16] P. Czajka, T. Gao, M. Hirschberger, P. Lampen-Kelley, A. Banerjee, J. Yan, D. G. Mandrus, S. E. Nagler, and N. P. Ong, *Oscillations of the Thermal Conductivity in the Spin-Liquid State of α -RuCl₃*, Nat. Phys. **17**, 915-919 (2021).
- [17] P. Czajka, T. Gao, M. Hirschberger, P. Lampen-Kelley, A. Banerjee, N. Quirk, D. G. Mandrus, S. E. Nagler, and N. P. Ong, *The Planar Thermal Hall Conductivity in the Kitaev Magnet α -RuCl₃*, ArXiv220107873 Cond-Mat (2022).
- [18] J. Nasu, *Thermal Transport in the Kitaev Model*, Phys. Rev. Lett. **119**, 127204 (2017).
- [19] T. Minakawa, Y. Murakami, A. Koga, and J. Nasu, *Majorana-Mediated Spin Transport in Kitaev Quantum Spin Liquids*, Phys. Rev. Lett. **125**, 047204 (2020).
- [20] J. a. N. Bruin, R. R. Claus, Y. Matsumoto, N. Kurita, H. Tanaka, and H. Takagi, *Robustness of the Thermal Hall Effect Close to Half-Quantization in α -RuCl₃*, Nat. Phys. **18**, 401-405 (2022).
- [21] D. Aasen et al., *Milestones Toward Majorana-Based Quantum Computing*, Phys. Rev. X **6**, 031016 (2016).
- [22] G. Kishony and E. Berg, *Converting Electrons into Emergent Fermions at a Superconductor--Kitaev Spin Liquid Interface*, Phys. Rev. B **104**, 235118 (2021).
- [23] M. G. Yamada and S. Fujimoto, *Electric Probe for the Toric Code Phase in Kitaev*

- Materials through the Hyperfine Interaction*, Phys. Rev. Lett. **127**, 047201 (2021).
- [24] R. G. Pereira and R. Egger, *Electrical Access to Ising Anyons in Kitaev Spin Liquids*, Phys. Rev. Lett. **125**, 227202 (2020).
- [25] D. Aasen, R. S. K. Mong, B. M. Hunt, D. Mandrus, and J. Alicea, *Electrical Probes of the Non-Abelian Spin Liquid in Kitaev Materials*, Phys. Rev. X **10**, 031014 (2020).
- [26] S.-Q. Jia, Y.-M. Quan, H.-Q. Lin, and L.-J. Zou, *Electron Tunneling Spectroscopy of the Kitaev Quantum Spin Liquid Sandwiched with Superconductors*, ArXiv210301003 Cond-Mat (2021).
- [27] M. Udagawa, S. Takayoshi, and T. Oka, *Scanning Tunneling Microscopy as a Single Majorana Detector of Kitaev's Chiral Spin Liquid*, Phys. Rev. Lett. **126**, 127201 (2021).
- [28] S. Biswas, Y. Li, S. M. Winter, J. Knolle, and R. Valentí, *Electronic Properties of α -RuCl₃ in Proximity to Graphene*, Phys. Rev. Lett. **123**, 237201 (2019).
- [29] J. Feldmeier, W. Natori, M. Knap, and J. Knolle, *Local Probes for Charge-Neutral Edge States in Two-Dimensional Quantum Magnets*, Phys. Rev. B **102**, 134423 (2020).
- [30] M. Carrega, I. J. Vera-Marun, and A. Principi, *Tunneling Spectroscopy as a Probe of Fractionalization in Two-Dimensional Magnetic Heterostructures*, Phys. Rev. B **102**, 085412 (2020).
- [31] E. J. König, M. T. Randeria, and B. Jäck, *Tunneling Spectroscopy of Quantum Spin Liquids*, Phys. Rev. Lett. **125**, 267206 (2020).
- [32] U. F. P. Seifert, T. Meng, and M. Vojta, *Fractionalized Fermi Liquids and Exotic Superconductivity in the Kitaev-Kondo Lattice*, Phys. Rev. B **97**, 085118 (2018).
- [33] W. Choi, *Topological Superconductivity in the Kondo-Kitaev Model*, Phys. Rev. B **98**, 155123(2018).
- [34] V. S. de Carvalho, R. M. P. Teixeira, H. Freire, and E. Miranda, *Odd-Frequency Pair Density Wave in the Kitaev-Kondo Lattice Model*, Phys. Rev. B **103**, 174512 (2021).
- [35] I. Pollini, *Electronic Properties of the Narrow-Band Material α -RuCl₃*, Phys. Rev. B **53**, 12769 (1996).
- [36] H.-S. Kim and H.-Y. Kee, *Crystal Structure and Magnetism in α -RuCl₃: An Ab Initio Study*, Phys. Rev. B **93**, 155143 (2016).
- [37] M. Ziatdinov et al., *Atomic-Scale Observation of Structural and Electronic Orders in the Layered Compound α -RuCl₃*, Nat. Commun. **7**, 13774 (2016).
- [38] L. J. Sandilands, Y. Tian, A. A. Reijnders, H.-S. Kim, K. W. Plumb, Y.-J. Kim, H.-Y. Kee, and K. S. Burch, *Spin-Orbit Excitations and Electronic Structure of the Putative Kitaev Magnet α -RuCl₃*, Phys. Rev. B **93**, 075144 (2016).
- [39] H. Y. Liu, Z. F. Hou, C. H. Hu, Y. Yang, and Z. Z. Zhu, *Electronic and Magnetic Properties of Fluorinated Graphene with Different Coverage of Fluorine*, J. Phys. Chem. C **116**, 18193 (2012).
- [40] R. D. Johnson et al., *Monoclinic Crystal Structure of α -RuCl₃ and the Zigzag Antiferromagnetic Ground State*, Phys. Rev. B **92**, 235119 (2015).
- [41] K. Bu, W. Zhang, Y. Fei, Z. Wu, Y. Zheng, J. Gao, X. Luo, Y.-P. Sun, and Y. Yin,

- Possible Strain Induced Mott Gap Collapse in 1T-TaS₂*, Commun. Phys. **2**, 146 (2019).
- [42] S. Mukherjee, N. F. Quackenbush, H. Paik, C. Schlueter, T.-L. Lee, D. G. Schlom, L. F. J. Piper, and W.-C. Lee, *Tuning a Strain-Induced Orbital Selective Mott Transition in Epitaxial VO₂*, Phys. Rev. B **93**, 241110 (2016).
- [43] T. Katase et al., *Breaking of Thermopower–Conductivity Trade-Off in LaTiO₃ Film around Mott Insulator to Metal Transition*, Adv. Sci. **8**, 2102097 (2021).
- [44] Y. Takahashi, T. Miyamachi, K. Ienaga, N. Kawamura, A. Ernst, and F. Komori, *Orbital Selectivity in Scanning Tunneling Microscopy: Distance-Dependent Tunneling Process Observed in Iron Nitride*, Phys. Rev. Lett. **116**, 056802 (2016).
- [45] D. J. Rizzo et al., *Charge-Transfer Plasmon Polaritons at Graphene/ α -RuCl₃ Interfaces*, Nano Lett. **20**, 8438 (2020).
- [46] B. Zhou, J. Balgley, P. Lampen-Kelley, J.-Q. Yan, D. G. Mandrus, and E. A. Henriksen, *Evidence for Charge Transfer and Proximate Magnetism in Graphene- α -RuCl₃ Heterostructures*, Phys. Rev. B **100**, 165426 (2019).
- [47] J. Tersoff and D. R. Hamann, *Theory and Application for the Scanning Tunneling Microscope*, Phys. Rev. Lett. **50**, 1998 (1983).

Supporting Information for:

Tunneling spectroscopic signatures of charge doping and Mott-phase transition in α - RuCl_3 in proximity to graphite

I. METHODS

In this work, we exfoliated the α - RuCl_3 thin films using the scotch tapes, from a bulk crystal synthesized by vacuum sublimation of commercial RuCl_3 powder. After repeatedly deduction of the film, we exfoliated again using a thermal release tap. Then, the thermal release tap with the α - RuCl_3 thin films was attached on a fresh surface of HOPG substrate. After heating the sample to 120 °C for 20 seconds in air condition, the α - RuCl_3 flakes were released on HOPG. Then the sample was annealed at 380 °C in ultra-high vacuum chamber (1E-10 Torr) in STM system for 2 hours for degassing, before STM/STS measurements. The STS spectra measurements were carried out using a lock-in technique at a frequency of 707 Hz and a modulation voltage in range from 5mV to 10 mV.

II. SUPPLEMENTAL FIGURES

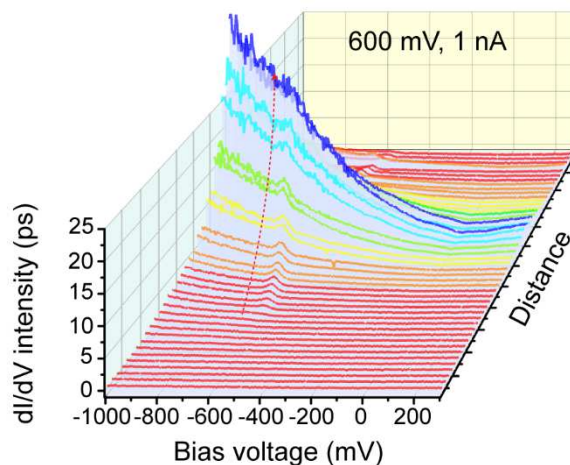


Fig. S1. dI/dV spectra collected along the green arrow line that is across the whole strain region in Fig. 2(a) in the main text, shows the evolution of the bandgap, where the insulating α - RuCl_3 evolves into a metallic form accompanied with the emerging of a peaked DOS around -600 meV from both sides (sample voltage=600mV, setpoint=1nA);

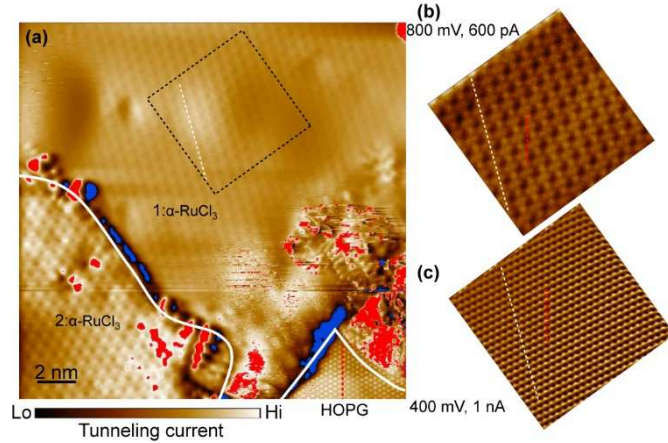


Fig. S2. Tip-surface distance dependent morphology evolution of STM images. **(a)** broad view STM image shows the single-layer (1: α -RuCl₃), bilayer α -RuCl₃(2: α -RuCl₃) and HOPG substrate. The lattice orientations in the three regions can be distinguished, where the white and red dashed lines show the lattice orientations of 1: α -RuCl₃ and graphite, respectively; **(b)** and **(c)** show the STM images acquired with different sample voltages and setpoint currents in region as squired in (a) on 1: α -RuCl₃. It shows the lattice in (b) fits well with the lattice of 1: α -RuCl₃, but it fits with the graphite lattice in (c) as decreasing the tip-surface distance, which confirms the tip-surface distance dependent STM morphology evolution on α -RuCl₃ has a closely related to the electron orbitals in the underneath graphite.

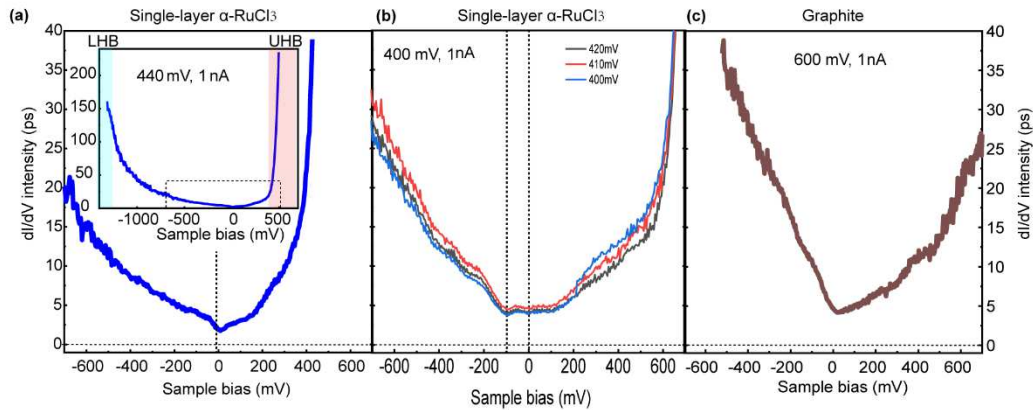


Fig. S3. dI/dV spectra on 1: α -RuCl₃ with **(a)** sample voltage of 440 mV and setpoint current of 1 nA. It shows a V-shaped point at the Fermi level. The view in a broad energy scale shows the Mott-gap regime is still distinguishable with the conservation of LHB and UHB similar as the bulk states; **(b)** sample voltage below 420 mV that is very closed to the band edge of UHB, setpoint current of 1 nA. It shows another V-shape minimal points below the Fermi level, which should contribute from the underneath graphite, and the shift of the Dirac point illustrates charge transfer from graphite to α -RuCl₃ happens. Furthermore, the shift of the band edge (inset in Fig. 3b in the main text) possibly induced by the band bending when the STM tip is very close to the surface of the heterostructure, **(c)** dI/dV spectrum collected from pristine graphite, which shows the Dirac point at the Fermi level.

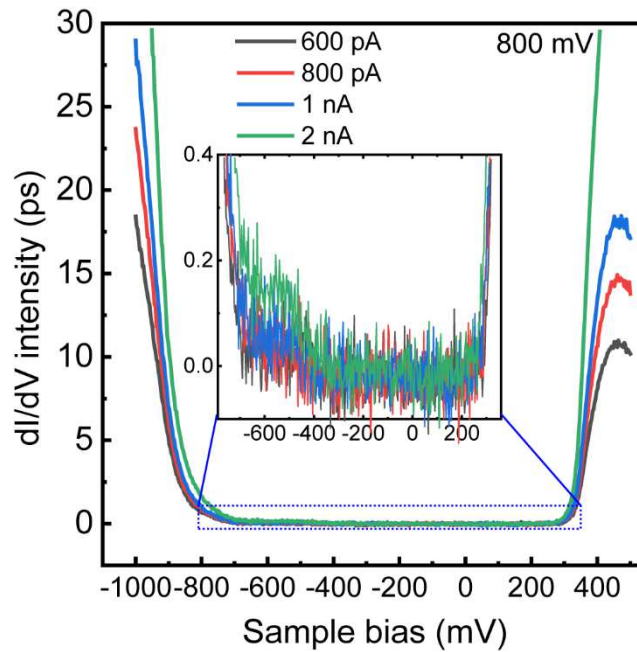


Fig. S4. dI/dV spectra acquired on 1: α - RuCl_3 with fixed sample voltages and variation of the setpoint current. As increasing of the setpoint current, the tip approaches to the surface, but the speed is more slowly than decreasing the sample voltage owing to the sharp conduction band edge. However, from the enlarged the dI/dV spectra, we can also observe the increased states in the Mott-gap, which means the tip-surface distance prominently decides whether the gap states can be detected or not.